Article:

eprints@whiterose.ac.uk
https://eprints.whiterose.ac.uk/

System-Level Investigation of Multi-MW Direct-Drive Wind Power PM Vernier Generators

DILEEP KUMAR KANA PADINHARU[1], GUANG-JIN LI[1], (Senior Member, IEEE), ZI-QIANG ZHU[1], (Fellow, IEEE), RICHARD CLARK[2], ARWYN THOMAS[2], and ZIAD AZAR[2]

[1]Department of Electronic and Electrical Engineering, The University of Sheffield, Sheffield, UK
[2]Siemens Gamesa Renewable Energy Limited, North Campus, Broad Lane, Sheffield, UK

Corresponding author: Guang-Jin Li (e-mail: g.li@sheffield.ac.uk).

ABSTRACT Surface mounted permanent magnet Vernier (SPM-V) machines are known for their high torque density but relatively poor power factor compared to conventional SPM machines. The high torque density feature of the SPM-V machines is desirable for direct-drive offshore wind power applications as it leads to reduced generator size, mass and cost. However, their poor power factor can negatively affect the converter cost and efficiency. This paper compares the system-level performance, including generator active and structural components and converter, between the SPM-V and the conventional SPM generator systems. Four different power ratings, i.e. 0.5MW, 3MW, 5MW and 10MW, have been considered to study the trend of system-level performance with increasing power rating. The study shows that the SPM-V generators can be lighter and cheaper than their conventional SPM counterparts. However, after the consideration of converter cost and efficiency, the conventional SPM generator exhibited slightly better overall performance. Nonetheless, with the development of novel Vernier topologies and reduction in converter costs in the future due to emerging technologies, the Vernier generators can still be competitive for direct-drive offshore wind power applications.

INDEX TERMS Direct-drive wind generator, power factor, system-level performance, Vernier machine.

NOMENCLATURE

Z	Number of stator slots
P_r	Number of rotor pole pairs
P_s	Number of stator winding pole pairs
EMF	Electromotive force (V)
E_{ph}	Phase EMF (V)
E_{ph-PU}	Normalized induced EMF
$Torque_{PU}$	Normalized torque
τ_r	Rotor pole pitch (m)
$\bar{\tau}_r$	Normalized rotor pole pitch
g	Mechanical airgap length (m)
h_m	Magnet thickness (m)
μ_{rec}	Magnet recoil permeability
V_{mag}	Total magnet volume (m³)
V_{mac}	Machine volume (m³)
α_p	Pole arc coefficient
k_w	Winding factor
T_{ph}	Series turns/phase
ω_m	Mechanical angular velocity (rad/s)
D_g	Airgap diameter (m)
L_{stk}	Stack length (m)
B_{P_r}	Fundamental radial airgap flux density (T)
K_{fl}	Magnet leakage factor
K_{ver}	Vernier factor
G_r	Gear ratio
Λ_1	Fundamental component of permeance function (H)
Λ_0	DC component of permeance function (H)
P	Active power (MW)
Q	Electrical loading (AT/m)
m	Number of phases
M_{tot}	Total generator mass (kg)
N	Mechanical speed (rpm)
M_{str}	Generator structural mass (kg)
p	Converter losses (kW)

I. INTRODUCTION

Direct-drive generators are a preferred choice for offshore wind power applications as they do not have the reliability and maintenance issues resulting from geared systems. However, with the trend of increasing power rating, the direct-drive generators are becoming bulkier due to the reduced turbine speed to maintain mechanical stability [1]. In the recent years, Vernier permanent magnet (PM) machines have attracted increasing interest for low speed direct-drive applications

because of their high torque density, inherent low torque ripple and relatively simple structure [2], [3]. But Vernier PM machines have a drawback of relatively low power factor compared to the conventional surface mounted PM (SPM) machines [4], [5]. The power factor becomes significantly lower (~0.4-0.5) for SPM Vernier (SPM-V) machines at high electrical loading, which is unavoidable for high power (multi-MW) offshore direct-drive generators [4]. This will result in a significant increase in converter rating and cost. But at the same time the direct-drive generators, because of their huge size, are going to contribute significantly to the overall cost and weight of the direct-drive powertrain system [6], [7]. Any reduction in the size (and mass) of the generator, due to the high torque density feature of the Vernier machines, is going to be beneficial. Therefore, it would be interesting and valuable to study the impact of high torque density but low power factor features of the Vernier machines on the overall system-level performance at multi-MW power level for offshore wind applications.

The existing research for SPM-V machines is largely limited to small-scale power levels (up to a few kWs). Recently, a few papers have been published for Vernier machines targeting at the system level study for wind applications. A system-level performance comparison between a 15kW conventional SPM and SPM-V wind power generators has been carried out in [5]. However, this power rating is considerably low to draw a meaningful conclusion. This is because, in the existing offshore wind market, the direct-drive generators often have multi-MW power ratings. Such large generators will have significantly higher electrical loadings and magnetic saturation levels. As a result, they might have even lower power factor, as investigated in [4]. Moreover, the comparison in [5] neglects the cost and mass of the generator structural materials, which have been found to dominate the total generator cost and mass at high power ratings [1]. Similarly, in [8] a rare-earth free Vernier generator with claw pole rotor design has been compared with a commercially available electrically excited synchronous generator (Enercon E-126, 7.5MW, 12rpm). This comparison takes the active and structural masses of the generator into consideration. However, the impact of the poor power factor on the converter cost and thereby the system-level cost has not been discussed.

To bridge this research gap, this paper makes the following contributions which also add to the novelty of this paper:

- Extending the system-level study of the SPM-V machine in comparison with the conventional SPM machine to multi-MW power levels. Four different power levels i.e. 0.5MW, 3MW, 5MW and 10MW have been considered.
- Considering both generator (active and structural materials) and power converter to compare the system-level cost and efficiency.

Different slot/pole number combinations have been considered for each power rating of the SPM-V machine to

select the optimal one for the final system-level comparison. A direct-drive generator with an outer rotor topology has been considered for this study. This is because it has advantages such as higher torque capability for low speed multi-pole structures and direct coupling between the generator rotor and the hub [9]. Moreover, the recent 10 MW wind generator developed for future wind energy research by the National Renewable Energy Laboratory (NREL) also adopts the outer rotor topology. The 2D model for a typical outer rotor conventional SPM machine with 12 stator slots (Z), 2 rotor pole pairs (P_r) and 2 stator winding pole pairs (P_s) is shown in FIGURE 1 (a). Similarly, the SPM-V machine with $Z = 12, P_r = 10, P_s = 2$ is shown in FIGURE 1 (b).
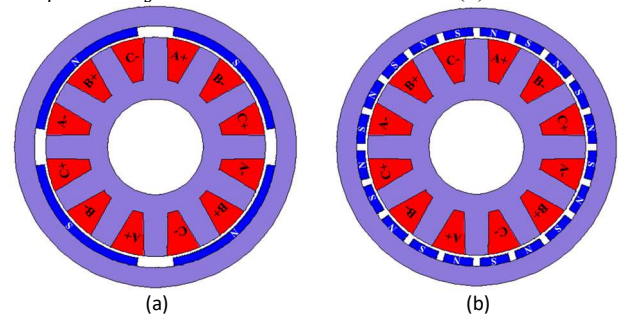

(a)   (b)

FIGURE 1. Examples of machines with outer rotors. (a) conventional SPM machine with $Z = 12, P_r = 2, P_s = 2$, and (b) SPM-V machine with $Z = 12, P_r = 10, P_s = 2$.

II. BASIC WORKING PRINCIPLE OF VERNIER MACHINES

The working principle of Vernier machines has been well documented in the literature [10]–[12]. In a conventional SPM machine, the fundamental harmonic of the armature field interacts with the fundamental harmonic of the PM field to produce electromagnetic torque. Therefore, in a conventional SPM machine, $P_r = P_s$. However, in an SPM-V machine, one of the slot harmonics $[(Z/P_s) \pm 1]$ of the armature field is made to interact with the fundamental rotor PM field to produce electromagnetic torque. As a result, the slot/pole number combinations of the SPM-V machines follow the rule governed by

$$P_r/P_s = (Z/P_s) \pm 1 \qquad (1)$$

The rotor pole pair is therefore given as

$$P_r = Z \pm P_s \qquad (2)$$

To get more insight, the SPM-V machine shown in FIGURE 1 (b) with $Z = 12, P_r = 10, P_s = 2$ is analyzed as an example. The stator has integer slot windings, meaning that the slot/pole/phase (SPP) equals to 1. The armature winding MMF harmonics can be predicted by 2D FEA using a slot-less stator with winding modeled as current sheet [11], as shown in FIGURE 2. It can be observed that, for this example, the slot harmonic order, $(Z/P_s) - 1 = 5$, is matched with the fundamental PM MMF harmonic order $P_r/P_s = 5$ to produce electromagnetic torque. Furthermore, unlike the conventional SPM machines, the SPM-V machines are generally designed

with open stator slots, as shown in FIGURE 1. When the slotting effect is considered, the fundamental winding MMF harmonic (harmonic order is 1) is modulated by the fundamental airgap permeance harmonic (harmonic order is 6). This leads to an additional modulated flux density harmonic (harmonic order is 6-1=5), as shown in FIGURE 2. This modulated harmonic component can represent a significant portion of the working harmonics. Therefore, the open slot structure is critical for the SPM-V machines to maximize their electromagnetic torque.
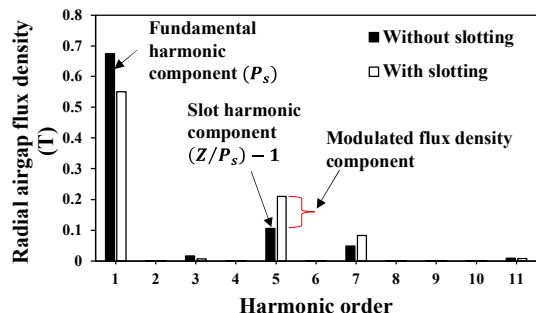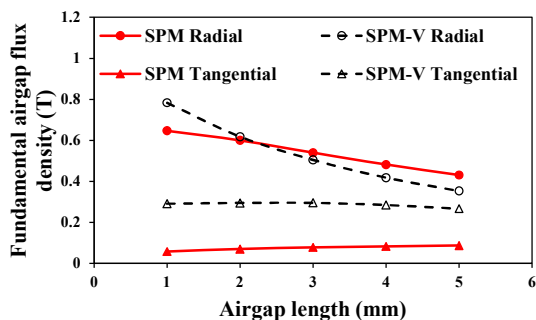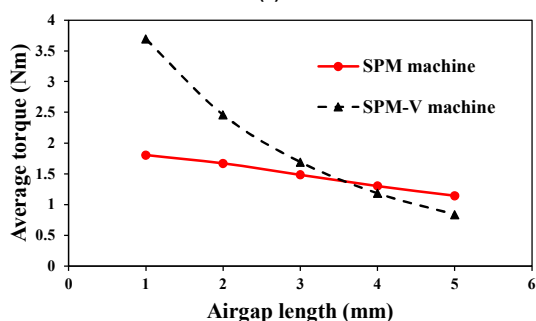

FIGURE 2. Comparison of radial airgap flux density spectra due to armature excitation of SPM-V machine with and without slotting effect.

It has been shown in the literature that the SPM-V machines can achieve higher torque density than the conventional SPM machines. To explain this, a conventional SPM machine as shown in FIGURE 1 (a) is taken as an example. The only difference between the conventional SPM machine and the SPM-V machine shown in FIGURE 1 is the rotor pole pair number.

(a)

(b)

FIGURE 3. Comparison between the conventional SPM and SPM-V machines in terms of (a) on-load fundamental radial and tangential airgap flux densities *vs* airgap lengths, and (b) average torques *vs* airgap lengths.

The on-load fundamental (the 1st order for the conventional SPM machine and the 5th order for the SPM-V machine) radial and tangential airgap flux densities are compared for different airgap lengths, as shown in FIGURE 3 (a). It is observed that the radial airgap flux densities are comparable between the two machines. However, the tangential airgap flux density of the SPM-V machine is almost 3 times that of the conventional SPM machine for all airgap lengths. The on-load torques produced by these two machines are shown in FIGURE 3 (b). Although the radial airgap flux density of the SPM-V machine becomes lower than the conventional SPM machine for airgap length > 2mm, the torque of the SPM-V machine can still be higher because of its higher tangential flux density [12]. Since the torque performance of the SPM-V machine is more sensitive to the airgap geometry (open stator slot and airgap length), selecting the right slot/pole number combination and airgap length will be very critical for achieving the optimal performance.

III. OPTIMAL SLOT/POLE NUMBER SELECTION

For the performance comparison, four different outer rotor conventional SPM machines with power ratings of 0.5MW [13], 3MW [14], 5MW and 10MW [15] are selected.

TABLE I. Key parameters of direct-drive generators

Generator key parameters				
Rated power (MW)	0.5	3	5	10
Rated speed (rpm)	32	15	14	10
Outer diameter (m)	2.195	5	6.5	10
Airgap length (mm)	2.15	5	6.5	10
Stack length (m)	0.55	1.2	1.5	1.8
Magnet volume (m^3)	0.016	0.227	0.345	0.92
Phase current (Arms)	530	2694	4436	8796
Electrical loading (AT/mm)	62.7	59	54.7	54.5
Turns/phase	133	56	42	32
Normalized pole pitch ($\overline{\tau}_r$)	9.5	5.3	3.5	3.4
Machine volume (m^3)	2	22.5	50	138
Machine/magnet volume ratio	123	99	144	150
Mass, cost and loss model for system-level analysis [15], [17]				
Mass density of steel core (kg/m^3)				7650
Mass density of magnet, NdFeB (kg/m^3)				7400
Mass density of copper (kg/m^3)				8940
Cost of steel core (€/kg)				2.5
Cost of magnet, NdFeB (€/kg)				50
Cost of copper (€/kg)				15
Cost of structural steel (€/kg)				2
Cost of generator side converter (€/kVA)				20
Cost of grid side converter (€/kVA)				20
Converter loss at rated power (%)				3

These reference machines from literature were originally designed for an inner rotor topology but have been converted to an outer rotor topology with the machine's overall outer diameter, the stack length, the magnet volume, the rotor speed and the airgap length being kept constant. The key parameters of the reference machines are given in TABLE I. The SPM-V machines are derived from their respective conventional SPM counterparts by changing the slot/pole number combinations,

which follow the rule in (2). It has been proven that, with an increasing gear ratio, the power factor of the SPM-V machines decreases [16]. Moreover, at high power level, the power factor tends to be poorer due to increased electrical loading. Hence a gear ratio of 5 (the minimum gear ratio to realize an integer slot winding) has been chosen for this study to achieve a reasonably good power factor.

Both the conventional SPM and SPM-V machines are globally optimized for maximum torque using the OPERA optimizer tool which uses a combination of deterministic and stochastic methods [17]. The geometric variables used for global optimization are the same as investigated in [4]. It is worth noting here that this paper adopts the same 2D FE model as in [4], which has already been experimentally validated using conventional SPM and SPM-V machine prototypes. The slot/pole number combinations used for different power ratings for the SPM-V machines are given in TABLE II. The electromagnetic performances for different slot/pole numbers and different power ratings are compared to select the optimal one for the system-level comparison in this paper.

A. EMF AND TORQUE COMPARISONS

To compare the induced EMF of the SPM-V machine (E_{ph-v}) against that of the conventional SPM machine (E_{ph-c}), the per-unit induced EMF (E_{ph-PU}) has been introduced, given as

$$E_{ph-PU} = \frac{E_{ph-v}}{E_{ph-c}} \tag{3}$$

For each power rating, E_{ph-c} is a constant and E_{ph-v} changes depending on the slot/pole number combination. To make the study more generic, the slot/pole number combinations of the SPM-V machines are represented as normalized pole pitch ($\bar{\tau}_r$) given by [4]

$$\bar{\tau}_r = \frac{\tau_r}{g + \dfrac{h_m}{\mu_{rec}}} \tag{4}$$

where τ_r is the rotor pole pitch, g is the mechanical airgap length, h_m and μ_{rec} are the magnet thickness and the recoil permeability, respectively.

The trend of E_{ph-PU} with $\bar{\tau}_r$ for different power ratings are shown in FIGURE 4 (a). As presented in [4], E_{ph-PU} of the SPM-V machine is found to be constant for a given $\bar{\tau}_r$. It is

worth noting that although an additional power rating of 5MW has been included in this study compared to [4], the conclusion remains the same. As the phase current for a given power rating is maintained the same between different slot/pole number combinations, $Torque_{PU}$ is expected to show a similar trend as E_{ph-PU}. The trends of $Torque_{PU}$ versus $\bar{\tau}_r$ for different power ratings are shown in FIGURE 4 (b). It is observed that because of saturation, $Torque_{PU}$ deviates slightly from the expected trend at high $\bar{\tau}_r$ (or low slot/pole numbers). The analysis shows that the SPM-V machine can achieve almost 60-65% higher torque than the conventional SPM machine at $\bar{\tau}_r$ between 6 and 7. However, for selecting the optimal slot/pole number combination, it is also important to compare the torque to mass and torque to cost ratios as will be investigated in the following section.
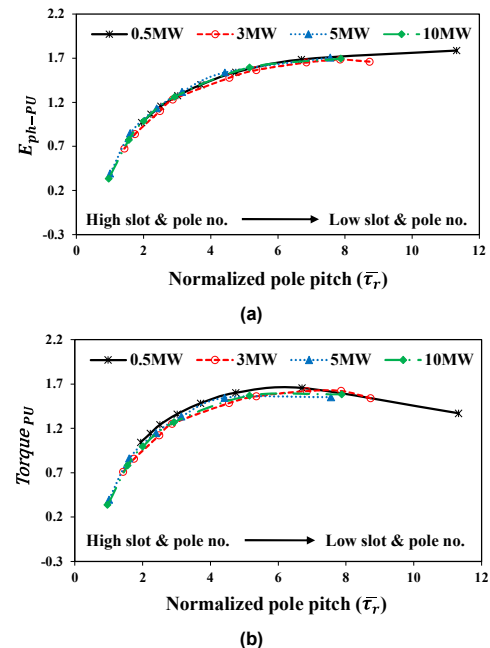

FIGURE 4. (a) E_{ph-PU} and (b) $Torque_{PU}$ of the SPM-V machine vs normalized pole pitch ($\bar{\tau}_r$) for different power ratings.

B. TORQUE/MASS AND TORQUE/COST COMPARISONS

The mass density and cost of the generator active materials used for the calculation of torque to mass (T2M) and torque to cost (T2C) ratios are given in TABLE I. The end winding

TABLE II. Slot/pole number combinations investigated in this paper

Machine Type	Design number	0.5MW			3MW			5MW			10MW		
		N_s	P_r	P_s	N_s	P_r	P_s	N_s	P_r	P_s	N_s	P_r	P_s
Conventional	0	294	49	49	480	80	80	864	144	144	960	160	160
Vernier	1	42	35	7	48	40	8	72	60	12	72	60	12
Vernier	2	84	70	14	60	50	10	144	120	24	120	100	20
Vernier	3	126	105	21	72	60	12	216	180	36	240	200	40
Vernier	4	168	140	28	96	80	16	288	240	44	360	300	60
Vernier	5	210	175	35	120	100	20	432	360	72	480	400	80
Vernier	6	252	210	42	192	160	32	864	720	144	960	800	160
Vernier	7	294	245	49	240	200	40	-	-	-	-	-	-
Vernier	8	-	-	-	360	300	60	-	-	-	-	-	-
Vernier	9	-	-	-	480	400	80	-	-	-	-	-	-

length is also considered for the calculation as it can be significantly longer at lower slot/pole number combinations for the SPM-V machines [17]. The end winding length for each turn is assumed to be twice the circumferential coil pitch length. Similar to the induced EMF and torque, T2M and T2C are also represented as normalized values using the mass and cost of their conventional machines as references. The comparison of normalized T2M and T2C of the SPM-V machines with slot/pole numbers and different power ratings are shown in FIGURE 5. The optimal T2M for the SPM-V machines is achieved at a $\bar{\tau}_r$ between 2.5 and 3. Whereas the T2C is optimal around $\bar{\tau}_r = 4$. For low slot/pole numbers, T2M and T2C are negatively impacted by core saturation, large back iron and longer end windings. Whereas for high slot/pole numbers, the poor torque performance results in low T2M and T2C.
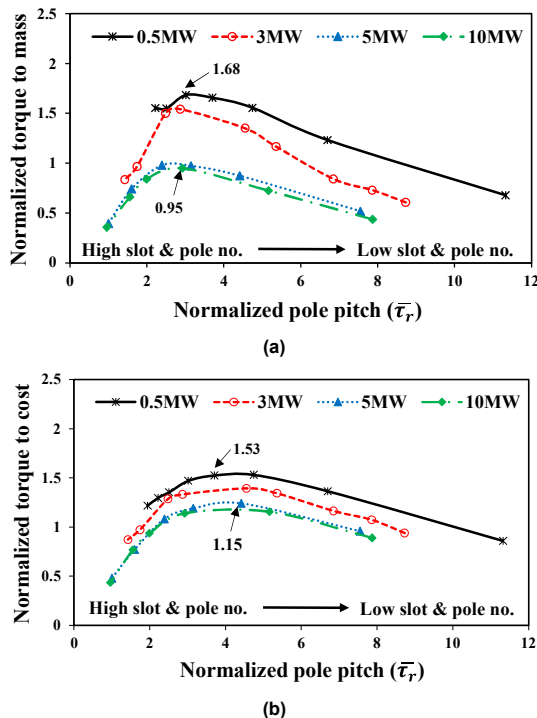

(a)

(b)

FIGURE 5. Normalized (a) T2M and (b) T2C of the SPM-V machines with different power ratings vs $\bar{\tau}_r$.

As an example, the absolute mass and cost of each active component of the 10MW generator are shown in FIGURE 6. Since the magnet and copper volumes (as the copper loss is constant) are maintained almost the same for a given power rating, the differences in T2M and T2C for different slot/pole number combinations are mainly driven by the volumes of the stator and rotor iron cores.
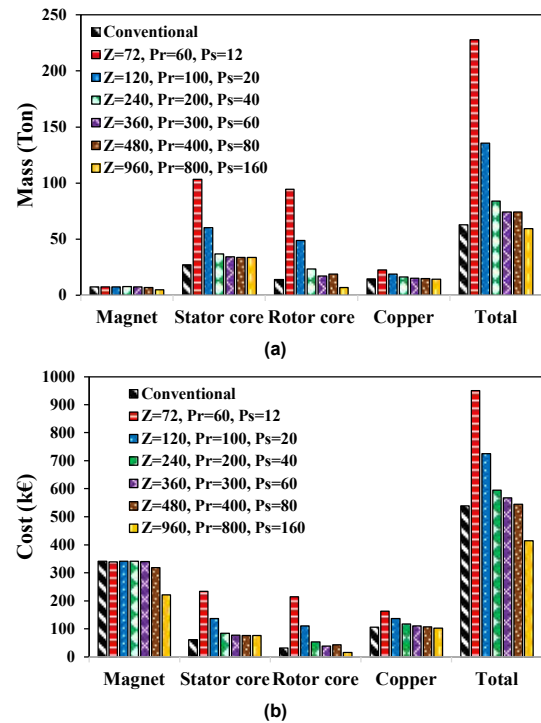

(a)

(b)

FIGURE 6. Comparison of (a) mass and (b) cost of 10MW generator active components between the conventional SPM and the SPM-V machines with different slot/pole numbers.

It is interesting to note that the benefits in normalized T2M and T2C diminish with increasing power rating. For example, at 0.5MW power level, the SPM-V machine can achieve a normalized T2M and T2C of 1.68 and 1.53, respectively. However, these values reduce to 0.95 and 1.15 respectively at 10MW power level. This can be explained as follows. The normalized pole pitches used for the reference conventional SPM machines are given in TABLE I. It can be observed that with increasing power rating, $\bar{\tau}_r$ decreases. This means that at high power rating, the conventional SPM machines are designed with relatively high slot/pole numbers. This is mainly due to the decreasing trend in the generator speed with power rating. Therefore, to maintain a reasonable output frequency at low speed, the rotor pole number needs to be high. Moreover, with increasing electrical loading (increasing power rating), a high stator slot number is favorable to increase the surface area for better heat dissipation. As a result, with high slot/pole numbers, the conventional SPM machines can reduce the back iron thickness significantly due to a reduced level of magnetic saturation, leading to reduced machine overall mass and cost. However, for the SPM-V machines to achieve their optimal performance, they still need to be designed at a $\bar{\tau}_r$ of around 3 with relatively thick back iron to avoid heavy magnetic saturation. Therefore, at higher power rating, the optimal SPM-V generators can be relatively heavier compared to conventional SPM generators.

C. Power Factor

Estimation of power factor is important to calculate the converter rating and cost. The power factor can be predicted

by 2D FEA analysis using the methodology developed in [18]. The end-winding inductance is also considered for the power factor calculation using the methodology developed in [19]. The comparison of power factors for the SPM-V machines with different $\bar{\tau}_r$ and different power ratings is shown in FIGURE 7.

TABLE III. Power factors of conventional SPM machines

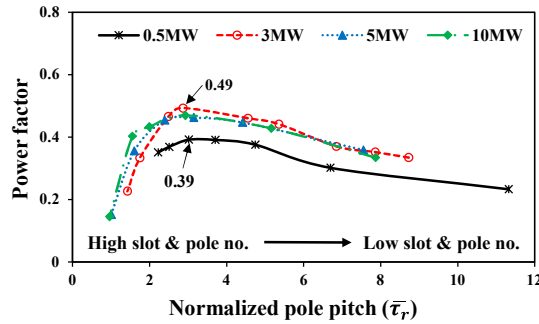|	0.5MW	3MW	5MW	10MW
Power factor	0.83	0.94	0.94	0.95

FIGURE 7. Power factor *vs* $\bar{\tau}_r$ of SPM-V machines with different power ratings.

It can be observed that the power factors of the SPM-V machines are relatively lower compared to their conventional counterparts which have near unity power factors, as shown in TABLE III. The power factor is found to be inversely proportional to electrical loading (see TABLE I) with the 0.5MW machine being the lowest [4]. For different slot/pole number combinations, it is found that the optimal power factors of the SPM-V machines are achieved when $\bar{\tau}_r$ is around 3. The high inter-pole leakage flux reduces the power factor at high slot/pole numbers. Whereas the long end winding and the core saturation results in the poor power factor for low slot/pole numbers.

D. Efficiency

For this study, only the electromagnetic losses (PM eddy current, iron and copper losses) have been considered for the efficiency calculation. It is observed that the Vernier machines in general have large PM eddy current loss [20]. This is because in the SPM-V machines the fundamental armature MMF is asynchronous with the rotor mechanical speed to utilize the modulation/gearing effect for torque generation. To reduce the eddy current loss, in this paper, the magnets have been circumferentially segmented into 4 segments for all the SPM-V machines. Also, both the conventional SPM and SPM-V machines at 0.5MW, 3MW, 5MW and 10MW have been axially segmented into 12, 26, 32 and 40 segments, respectively. The impact of axial segmentation on PM eddy current loss is estimated using a correction factor calculated in [21].
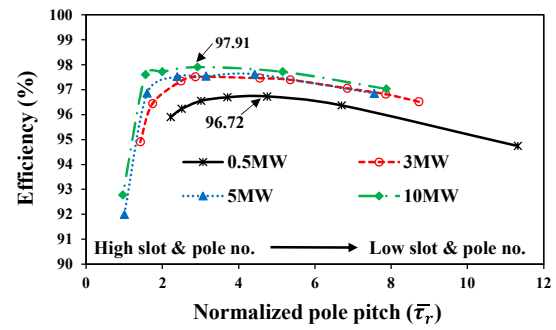

FIGURE 8. Efficiency *vs* $\bar{\tau}_r$ for SPM-V machines with different power ratings.

The comparison of efficiency versus $\bar{\tau}_r$ for the SPM-V machines with different power ratings are shown in FIGURE 8. The optimal efficiencies for the SPM-V machines are achieved when $\bar{\tau}_r$ is between 3 and 4. The maximum efficiencies of the SPM-V machines are compared with the conventional SPM machines at each power rating and are given in TABLE IV.

TABLE IV. Efficiency comparison between the conventional SPM and SPM-V machines

	0.5MW	3MW	5MW	10MW
Conventional SPM	96.26	97.4	97.47	97.94
SPM-V (max value)	96.72	97.52	97.62	97.91

For example, the electromagnetic losses of the 10MW conventional SPM machine are compared with the SPM-V machines with different slot/pole number combinations, as shown in FIGURE 9. It is found that the PM eddy current loss, because of segmentation, is negligible compared to other losses. However, the copper loss increases for lower slot/pole numbers due to longer end windings. The total iron losses (including stator and rotor core losses) is observed to increase for both low and high slot/pole numbers. This is mainly due to high armature flux density towards low slot/pole numbers and high operating frequency towards high slot/pole numbers [17].
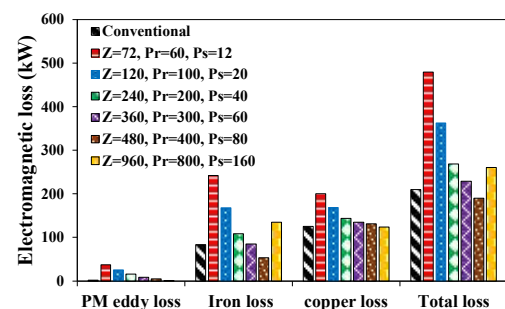

FIGURE 9. Comparison of losses between the 10MW conventional SPM and SPM-V machines with different slot/pole numbers.

Based on the above comparison of overall performances, the optimal slot/pole number combinations have been selected for the SPM-V machines with different power ratings, as shown in TABLE V.

TABLE V. Optimal slot/pole numbers selected for the SPM-V machines with different power ratings

Power rating	Slot/pole numbers	Normalized pole pitch ($\bar{\tau}_r$)
0.5MW	$Z = 210, P_r = 175, P_s = 35$	3
3MW	$Z = 192, P_r = 160, P_s = 32$	2.9
5MW	$Z = 216, P_r = 180, P_s = 36$	3.1
10MW	$Z = 240, P_r = 200, P_s = 40$	2.9

It is found that the optimal performance of the SPM-V machines is achieved when $\bar{\tau}_r$ is around 3 for all the power ratings. It is also interesting to note that at this $\bar{\tau}_r$, the slot/pole number combinations are very much similar even for a wide range of power ratings. This can be explained as follows. $\bar{\tau}_r$ in (4) can be represented as (see APPENDIX for more details)

$$\bar{\tau}_r = \frac{\pi/(2P_r)}{0.001 + \left(\frac{V_{mag}}{V_{mac}}\right)\frac{1}{4\alpha_p\mu_{rec}}} \quad (5)$$

where V_{mag} and V_{mac} are the magnet and machine volumes, respectively, α_p is the pole arc coefficient defined as the ratio of magnet arc (w_m) to rotor pole pitch (τ_r). The value of α_p, as shown in FIGURE 10, is almost 1 at $\bar{\tau}_r= 3$ for all power ratings. The ratios of machine volume to magnet volume for different power ratings are shown in TABLE I and range from 100 to 150. The rotor pole pair number (P_r) for these ranges of V_{mac}/V_{mag} when $\bar{\tau}_r= 3$ can be calculated using (5). It is observed that P_r varies through a relatively narrow range from around 145 to 200 as shown in FIGURE 11.
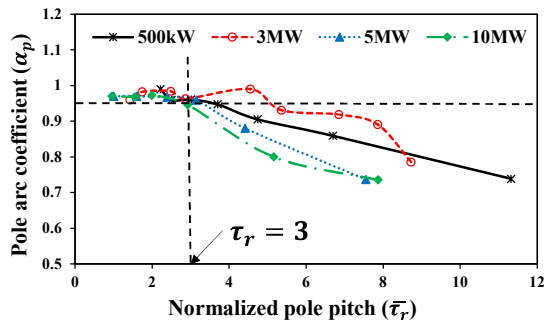

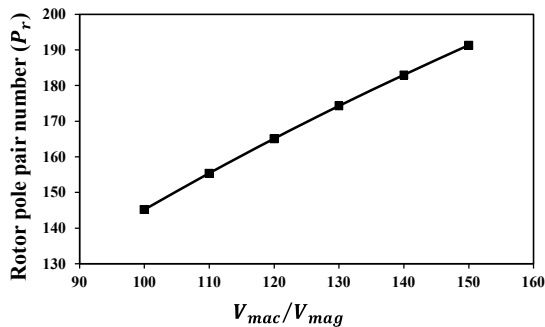FIGURE 10. α_p vs $\bar{\tau}_r$ for SPM-V machines with different power ratings.

FIGURE 11. Rotor pole pair number calculated using (5) for different V_{mac}/V_{mag} when $\bar{\tau}_r$= 3.

Therefore, a $\bar{\tau}_r$ of around 3 or P_r within the above mentioned ranges is a good design option as it allows the SPM-V machines to achieve good overall performance.

IV. FINAL DESIGN FOR SPM-V MACHINE FOR SYSTEM-LEVEL COMPARISON

When $\bar{\tau}_r$=3, the torque capability of the SPM-V machine is observed to be much higher than the conventional SPM machine. However, for the system-level comparison, both the conventional SPM and SPM-V machines will be compared at the same power rating. Redesigning the SPM-V machine (at $\bar{\tau}_r$=3) to make the power rating the same as the conventional SPM machine requires the understanding of the power equation, which is discussed as follows.

The analytical equation for the induced EMF (E_{ph-v}) of the SPM-V machine is given by [4]

$$E_{ph-v} = \frac{k_w T_{ph}\omega_m D_g L_{stk} B_{P_r} K_{fl}}{\sqrt{2}}(K_{ver} + 1) \quad (6)$$

where k_w is the fundamental winding factor, T_{ph} is the number of series turns per phase, ω_m is the rotor mechanical angular velocity, D_g and L_{stk} are the airgap diameter and the stack length, respectively, B_{P_r} is the magnitude of the fundamental radial airgap flux density created by rotor magnets with P_r pole pair, K_{fl} is the PM leakage factor, K_{ver} is the Vernier factor defined as

$$K_{ver} = \frac{G_r^2}{(2G_r+1)}\frac{\Lambda_1}{\Lambda_0} \quad (7)$$

where Λ_0 is the DC component and Λ_1 is the peak value of the fundamental component of the airgap permeance function.

The generic equation of active power (P_v) for an m-phase machine carrying a phase current of I_{ph} is given by

$$P_v = mE_{ph-v}I_{ph} \quad (8)$$

Substituting (6) in (8) and expressing I_{ph} in terms of electrical loading (Q), i.e. $I_{ph} = \frac{\pi D_g Q}{2mT_{ph}}$, the power equation for an SPM-V machine can be written as

$$P_v = (\omega_m)\left(\frac{\pi D_g^2 L_{stk}}{4}\right)(B_{P_r}Q)[\sqrt{2}k_w K_{fl}(K_{ver} + 1)] \quad (9)$$

The power equation has 4 major terms. The first term (ω_m) refers to the angular mechanical speed, the second term ($\pi D_g^2 L_{stk}/4$) refers to the machine volume, the third term ($B_{P_r}Q$) denotes the product of electrical loading and magnetic loading and the final term $[\sqrt{2}k_w K_{fl}(K_{ver} + 1)]$, a unique term for Vernier machines, incorporates the airgap permeance, the gear ratio and the leakage factor according to a specific normalized pole pitch [4].

From (9), the active power is observed to be proportional to the volume of the machine. Hence, for the same power rating as a conventional SPM machine, the SPM-V machine can be designed with reduced machine volume (and mass). This can be achieved by either reducing the axial length of the machine or reducing its outer diameter as shown in (9). It is worth

noting that wind generators often have relatively large diameters compared to their axial lengths. Therefore, massive supporting structures are required to provide enough stiffness between the stator and rotor to maintain a small airgap required for high torque/power density. The mass and cost of the inactive/supporting structure are largely driven by the diameter of the machine with high power ratings [22]. A reduced outer diameter for the SPM-V machine can be more favorable for reducing the overall generator mass. Hence, in this paper, the SPM-V machines are redesigned with a reduced outer diameter for the final system-level comparison. The step by step approach for achieving the final design of the SPM-V machines is as explained below.

- $\bar{\tau}_r$ for the new design of the SPM-V machine is maintained the same as the optimal one shown in TABLE V. The new diameter (D_{g-new}) can be derived from the original diameter (D_g) using (9) as

$$\frac{P_c}{P_v} = \frac{D_{g-new}^2}{D_g^2} \qquad (10)$$

where P_c is the active power of the conventional SPM machine.

- The new airgap length (g_{new}) can be calculated by

$$g_{new} = \frac{D_{g-new}}{1000} \qquad (11)$$

- Similar to the conventional SPM machine, the terminal voltage is designed to be <690V. Hence, the series turns per phase (T_{ph-ne}) is adjusted accordingly.
- The ratio V_{mac}/V_{mag} is maintained the same according to (5) and hence the magnet volume required for the new design is proportionally reduced.
- As the electrical loading is assumed to be the same, the new I_{ph-n} can be approximately calculated as

$$I_{ph-new} = \frac{\pi D_{g-new} Q}{2m T_{ph-new}} \qquad (12)$$

With the major parameters available, the machines are then globally optimized for achieving maximum torque. The current density in the SPM-V machine is kept the same as the conventional SPM machine to have a similar thermal performance. The final design and the system-level performance comparison between the SPM-V generators and the conventional SPM generators for wind power applications are discussed in section V and VI.

V. ELECTROMAGNETIC PERFORMANCE COMPARISON FOR THE FINAL DESIGN

The key parameters of the final designs of the SPM-V generators for different power ratings in comparison with the conventional SPM generators are shown in TABLE VI. Because of the increased torque capability of the SPM-V generators, their outer diameters are nearly 10-16% smaller than their SPM counterparts with the same power ratings. This results in reducing the machine and magnet volumes of the

SPM-V generators by 19-29%. For comparing the generator characteristics between the two machines, the 10MW power level has been chosen as an example.
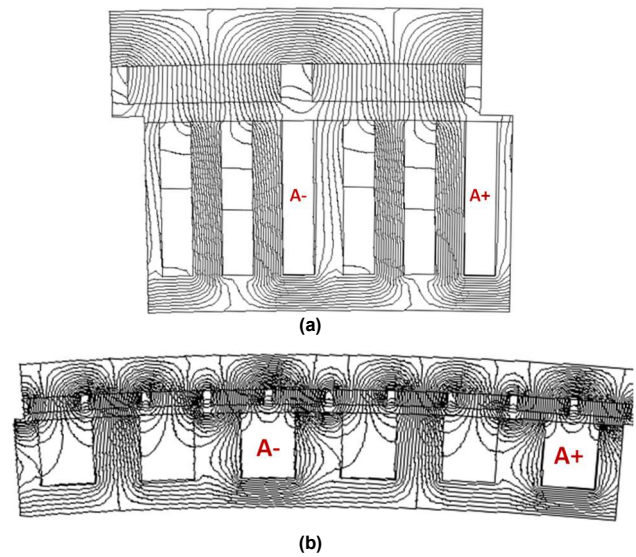
FIGURE 12. Open circuit flux distribution comparison between 10MW (a) conventional SPM and (b) SPM-V generators.

The one pole pair models for the 10MW conventional SPM and SPM-V generators with their open-circuit flux distributions (with phase A having the maximum flux linkage) are shown in FIGURE 12. It can be observed that, although the SPM-V generator has 5 rotor pole pairs, due to the flux modulation effect, there will be only one stator pole pair.

FIGURE 13. Comparison of open-circuit induced EMF and line-line terminal voltage (a) waveforms (b) spectra between the conventional SPM and SPM-V 10MW generators.

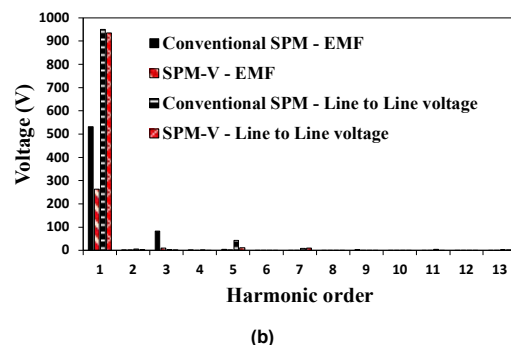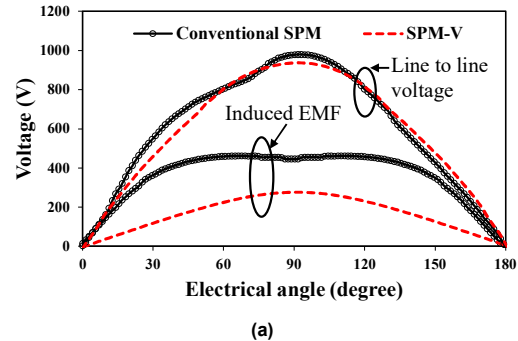**TABLE VI. System-level cost, weight and efficiency comparisons between conventional SPM and SPM-V machines**

Rated power	0.5MW		3MW		5MW		10MW	
Machine type	Conventional SPM	SPM-V	Conventional SPM	SPM-V	Conventional SPM	SPM-V	Conventional SPM	SPM-V
Generator key parameters								
Rotor outer diameter (m)	2.195	1.9	5	4.5	6.5	5.5	10	9
Airgap length, g (mm)	2.15	1.9	5	4.5	6.5	5.5	10	9
Stator yoke height, h_{ys} (mm)	17.5	11.2	21	22	17.1	30	19	33
Stator tooth height, h_t (mm)	82	51.7	79.5	67.7	64.4	64.2	81	74.3
Stator slot pitch, τ_s (mm)	22.9	27.9	32.15	72.2	23.3	78.7	32.3	116
Rotor yoke height, h_{yr} (mm)	17.6	11.6	24.7	26.3	17.6	28.6	29	40
Magnet thickness, h_m (mm)	5.4	3.85	14.2	12.1	14.2	10.1	20	17
Magnet width, w_m (mm)	55.7	16.5	83.3	40	56.2	45	80.5	60.5
Magnet volume, V_{mag} (m³)	0.016	0.012	0.227	0.186	0.345	0.245	0.92	0.74
Phase current, I_{ph} (Arms)	530	1116	2695	5201	4436	9170	8973.5	18012
Number of turns/phase, T_{ph}	133	55	56	26	42	18	32	14
Number of turns/coil	19	11	14	13	7	9	8	7
Number of parallel circuits	7	7	20	16	24	18	40	20
Power factor	0.83	0.41	0.94	0.51	0.94	0.46	0.95	0.49
MVA rating	0.65	1.3	3.24	6	5.3	11	10.5	20.3
Generator weight (Ton)								
Iron	2.5	1.2	13.7	11	16.6	18.5	40.8	44.9
Copper	0.8	0.65	4.2	4.2	6.3	6.2	14.6	14.1
PM	0.1	0.1	1.8	1.5	2.8	2	7.5	6
Generator active material	**3.4**	**1.9**	**19.7**	**16.7**	**25.7**	**26.7**	**62.9**	**65**
Generator structure	**5.2**	**4.5**	**56**	**50.4**	**104.8**	**88.7**	**246.1**	**221.5**
Total generator mass	**8.6**	**6.4**	**75.7**	**67.1**	**130.5**	**115.4**	**309**	**286.5**
System-level cost (k€)								
Generator active material	17.5	11.9	145.6	124.1	210.4	177.6	538.8	478.4
Generator construction	10.4	9	112	100.8	209.7	177.5	492	443
Total generator cost	**27.9**	**20.9**	**257.6**	**224.9**	**420.1**	**355.1**	**1031**	**921.3**
Converter– generator side	13	26	64.8	120	106	220	210	406
Converter – grid side	10	10	60	60	100	100	200	200
Total converter cost	**23**	**36**	**124.8**	**180**	**206**	**320**	**410**	**606**
Total system cost	**50.9**	**56.9**	**382.4**	**404.9**	**626.1**	**675.1**	**1441**	**1527.3**
Efficiency								
Generator efficiency (%)	**96.26**	**96.1**	**97.4**	**97.32**	**97.46**	**97.3**	**97.94**	**97.86**
Converter efficiency (%)	**97**	**94.3**	**97**	**94.8**	**97**	**94.4**	**97**	**94.56**
System efficiency (%)	**93.4**	**90.6**	**94.4**	**92.2**	**94.5**	**91.8**	**95**	**92.5**

For the same terminal voltage (690V), the induced EMF of the SPM-V generator is much lower than the conventional SPM generator as shown in FIGURE 13(a). This suggests that the reactive power in the SPM-V generator is quite large compared to the conventional SPM generator and thereby resulting in poor power factor. However, compared to the conventional SPM generator, the voltage quality of the SPM-V generator is much better with nearly sinusoidal waveform. The poor voltage quality in the conventional SPM generator is due to higher 3rd and 5th harmonic components in the induced EMF and line-line voltage, as shown in FIGURE 13(b). The torque waveform comparison between the 10MW conventional SPM and SPM-V generators is shown in FIGURE 14(a). It is observed that the SPM-V generator has a significantly lower torque ripple compared to the conventional SPM generator. The torque spectra shown in FIGURE 14(b) reveals that the torque ripple is largely dominated by the 6th harmonic, which is due to the high cogging torque component.
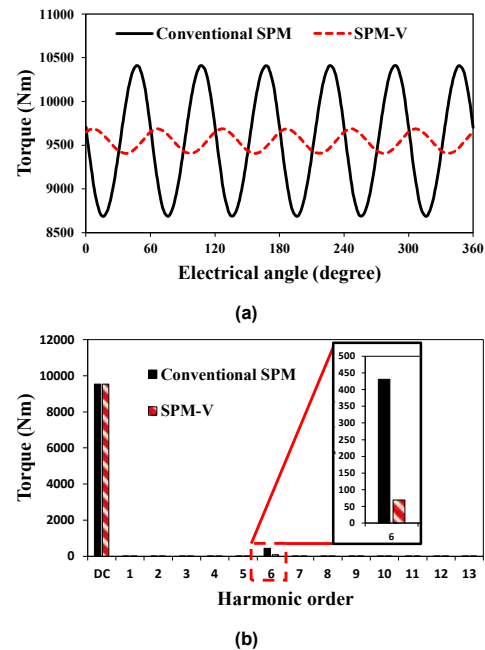

(a)

(b)

FIGURE 14. Comparison of (a) torque waveforms (b) torque spectra between the conventional SPM and SPM-V 10MW generators.

The torque ripple coefficient [(ratio of peak-peak torque to average torque)×100] and cogging torque ratio [(ratio of peak-peak cogging torque to average torque)×100] comparison for different power ratings between the two generator types is shown in TABLE VII. For different power ratings, the torque ripple coefficient and the cogging torque ratios of the SPM-V generators are consistently lower compared to the conventional SPM generator. It is worth noting here that no cogging torque reduction techniques like magnet shaping, skewing, etc. have been used for both generators. The torque ripple coefficients for the conventional generator are higher than the typical values, as the generator designs are not globally optimized to minimize the torque ripple. The low cogging torque for the SPM-V generator is due to their relatively high value of Least Common Multiple (LCM) between Z and $2P_r$ [23].

TABLE VII. Comparison of torque ripple coefficients and cogging torque ratios between the conventional SPM and SPM-V generators with different power ratings

	0.5MW	3MW	5MW	10MW
Cogging torque ratio (%)				
Conventional SPM	38	37	13	15
SPM-V	4.7	5	7.3	3
Torque ripple coefficient (%)				
Conventional SPM	36	42	17	18
SPM-V	6	6	8.7	3.7

VI. SYSTEM-LEVEL COMPARISON AND DISCUSSION

Because of the poor power factor of the SPM-V generators, their MVA ratings and phase currents are almost doubled compared to the conventional SPM generators. This will have detrimental effects on the converter cost and efficiency. Therefore, for a fairer comparison, the generator and the converter costs have to be combined to compare the overall system-level performance between these two types of machines.

A. GENERATOR MASS AND COST

The active material mass and cost of the generator can be calculated as described in section III.B. However, for high power direct-drive wind generators, the consideration of the structural mass and cost is also very critical. It is estimated that the structural mass of a 5MW direct-drive generator can account for 80% of the overall generator mass [24]. There are different methods used in literature to calculate the structural mass of the generator [25], [26]. However, most of these calculations require a detailed analysis of the forces in the airgap and the resultant deformations in the structural components. A relatively simple equation [as described by (13)] has been presented in [27] for the calculation of the total mass (M_{tot} including active and structural masses) of the direct-drive generators.

$$M_{tot} = 97.7 \frac{P}{\sqrt{N}} \qquad (13)$$

where P is the rated power (MW) and N is the rated speed (rpm).

This analytical model was developed by curve fitting the data of over 90 commercially available offshore wind generators (including both geared and direct-drive ones). Moreover, the analytical model has proven its accuracy in predicting the mass of direct-drive multi-MW generators [27]. Hence in this paper, this simple analytical model has been adopted for calculating the total mass of the conventional SPM generators. However, this equation cannot take into account the impact of reduced diameter on the mass of the SPM-V generators, which needs to be calculated using the following method:

- The structural mass of the conventional SPM generators can be obtained by subtracting the active mass from the total generator mass calculated using (13).
- A simple generator structural model with a cylinder connected to the shaft by arms is assumed for both the stator and the rotor [24]. It is shown that the length of the arms (in the radial direction) doubles when the machine diameter doubles [26]. The cylinder mass is also proportional to the machine diameter. Since the axial length of the SPM-V generator is the same as the conventional SPM generator, it is assumed that the structural mass is proportional to the diameter of the machine. Hence, the structural mass of the SPM-V generators (M_{str_v}) can be calculated based on the structural mass of the conventional SPM generators (M_{str_c}) as

$$M_{str\_v} = M_{str\_c} \frac{D_{g\_v}}{D_{g\_c}} \qquad (14)$$

where D_{g_c} and D_{g_v} are the outer diameters of conventional SPM and SPM-V generators, respectively.

- The total mass of the SPM-V generator can be obtained by adding the active mass to the structural mass obtained from (14).

The structural cost of the generator is calculated using the structural steel cost as given in TABLE I. The final comparison of generator mass and cost between the conventional SPM and SPM-V generators with different power ratings are shown in TABLE VI. The trends of total generator mass for a direct-drive conventional SPM generator along with its active and structural mass contributions are shown in FIGURE 15. It can be observed that the structural mass highly dominates the total generator mass for the range of power ratings considered in this paper. The rate of increase in total generator mass from 5MW to 10MW is higher than the increase in power rating itself. The contribution of structural mass increases from 60% to 80% from 0.5MW to 10MW.
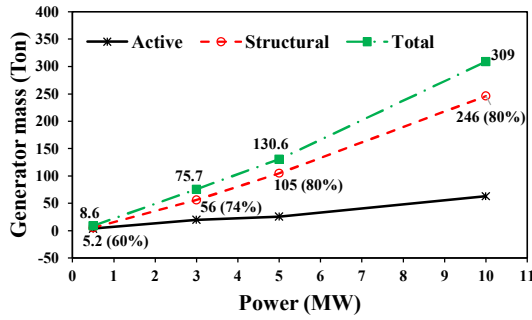
FIGURE 15. Trends of active, structural and total generator masses with increasing power rating for the direct-drive conventional SPM generators.
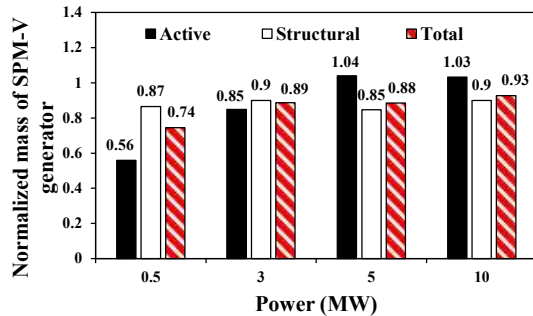

FIGURE 16. Normalized active, structural and total masses of the SPM-V generators with reference to those of the SPM generators at different power ratings.

To ease the comparison of generator mass between the SPM-V and conventional SPM generators, the normalized mass has been used. The active, structural and total masses of the conventional SPM generators at each power rating are taken as the reference for calculating this normalized masses of the SPM-V generators, as shown in FIGURE 16. It is observed that the active mass of the SPM-V generator can be 44% lighter than the conventional SPM generator at 0.5MW power level. However, this gain diminishes with increasing power rating and at 10 MW power level, the active mass of the SPM-V generator can be 3% heavier than its conventional counterpart. The reason for this trend has been explained in section III.B. However, because of the higher torque capability of the SPM-V generators, their structural mass could be reduced by 10-14%, which is proportional to the reduction in the outer diameter. Therefore, the total mass of the SPM-V generator is lighter, by 26% and 7% at 0.5MW and 10MW power levels, respectively.

The trends of the active, structural and total generator costs with increasing power ratings for the conventional SPMs are shown in FIGURE 17. Unlike the generator mass, both the active and structural costs contribute almost equally to the total generator cost. Similar to the generator mass, a normalized cost of the SPM-V generator is shown in FIGURE 18. There is almost a 32% cost reduction in the active component of the SPM-V generator at 0.5 MW power level in comparison with its conventional counterpart. However, the rate of reduction decreases with the increasing power rating, and at 10MW power level, the cost reduction is around 11%. The structural cost reduction of the SPM-V generator follows the trend of its

structural mass reduction. Overall, it is found that a direct-drive SPM-V generator costs 25% and 10% less than its conventional SPM counterpart at 0.5MW and 10MW power levels, respectively. However, the poor power factor of the SPM-V generator will increase the rating and cost of the converter and could lead to increased overall system-level cost compared to the conventional SPM generator. Therefore, the converter cost is further calculated, and the system-level performance comparison is presented in the next section.
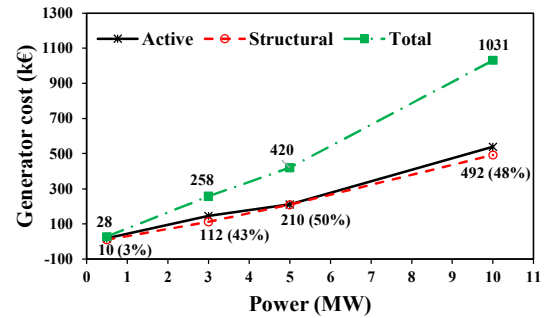

FIGURE 17. Trends of active material, structural and total generator costs with increasing power rating for the conventional direct-drive SPM generators.
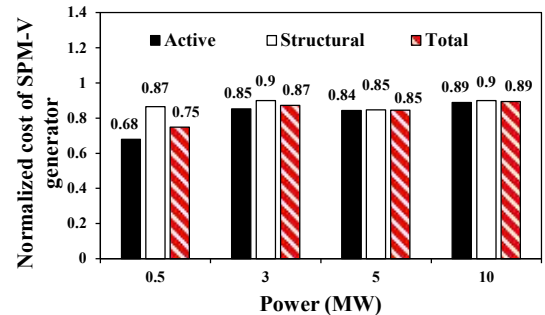

FIGURE 18. Normalized active, structural and total costs of the SPM-V generators with reference to those of the SPM generators at different power ratings.

A. SYSTEM-LEVEL COST AND EFFICIENCY COMPARISONS

A back-to-back converter with a DC-link is assumed to be the interface between the generator and the grid [15]. It is worth noting that the grid side converter is unaffected by the generator power factor/MVA rating. Therefore, only the cost of the generator side converter is scaled up/down according to the power factor/MVA rating. TABLE VI shows the power factor comparison between the SPM-V and conventional SPM generators. Due to the poor power factors (~0.5), the MVA ratings of the SPM-V generators are almost doubled compared with the conventional SPM generators. The cost models of the generator side and grid side converters have been given in TABLE I. The calculated converter costs for both the SPM-V and conventional SPM generators for different power ratings are listed in TABLE VI. The contributions of the converter and generator costs to the total system costs for the conventional SPM generators are shown in FIGURE 19. It is observed that with an increasing power rating the contribution of the

generator cost also increases, to almost 72% at 10MW power level.

The normalized generator, converter and total system costs of the SPM-V generators are shown in FIGURE 20.
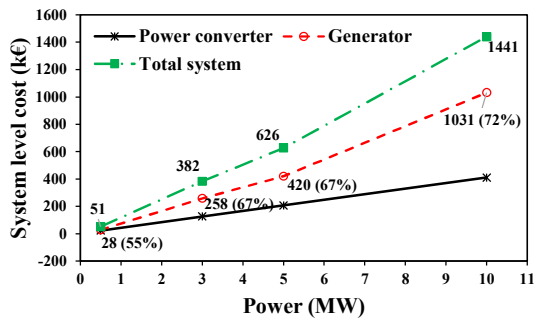

FIGURE 19. Contributions of converter and generator costs to the total system cost at different power ratings.
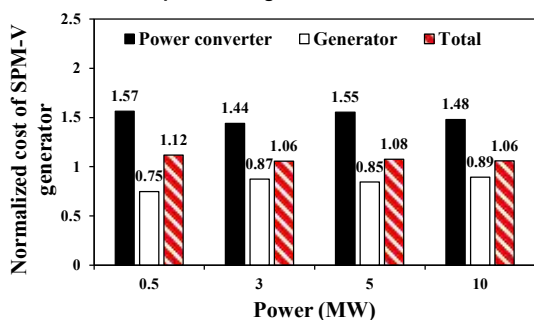

FIGURE 20. Normalized converter, generator and total system costs of the SPM-V generators with reference to those of the SPM generators at different power ratings.

It is observed that, due to the poor power factors of the SPM-V generators, their converter costs have been increased by almost 50% compared to the conventional SPM generators with different power ratings. However, the machine cost reductions for the SPM-V generators, as discussed earlier, are only about 10-25%. Therefore, from an overall system-level point of view, the SPM-V generator systems still cost more (by 12% at 0.5MW and 6% at 10MW) than their conventional SPM counterparts.

The efficiencies predicted by using 2D FEA for the conventional SPM and SPM-V generators with different power ratings are also listed in TABLE VI. It is observed that the efficiencies of the SPM-V generators are comparable to that of the conventional SPM generators at all power ratings. Assuming that the grid side converters of the conventional SPM and SPM-V generator systems have the same current, the converter loss of the SPM-V generator system can be calculated as [14]

$$p_v = \frac{p_c}{31}\left(1 + 10\frac{I_{ph-v}}{I_{ph-c}} + 5\frac{I_{ph-v}^2}{I_{ph-c}^2} + 15\right) \quad (15)$$

where p_c are the converter losses of the conventional SPM generators (assumed 3% of the rated power across the power

ratings [15]), I_{ph-v} and I_{ph-c} are the rated phase currents of the SPM-V and conventional SPM generators, respectively.

The calculated power converter efficiencies are compared between the conventional SPM and SPM-V generator systems and are shown in TABLE VI. Since the generator side converters have high currents, the efficiencies of the converters for the SPM-V generator systems can be 2-3% lower than that of the conventional SPM generators. Therefore, the system-level efficiencies of the SPM-V generator systems, calculated as the product of generator and converter efficiencies, are lower than the conventional SPM systems.

VI. CONCLUSION

A system-level performance comparison between the conventional SPM and SPM-V generators has been carried out for direct-drive offshore wind power applications. The study shows that the mass of a direct-drive generator is highly dominated by the structural mass (nearly 80%) rather than by the active mass at high power ratings (5-10MW). However, the generator cost has comparable contributions from both the active and structural components. The SPM-V generators can be lighter (26% at 0.5MW and 7% at 10MW) and cheaper (25% at 0.5MW and 11% at 10MW) than the conventional SPM generators. But the increased converter cost due to the poor power factor makes the SPM-V generator system more costly (12% at 0.5MW and 6% at 10MW) than the conventional SPM generator systems. Moreover, the poor power factor also reduces the system efficiency of the SPM-V generator systems by 2-3% compared with the conventional SPM generator systems. Overall, the conventional SPM generator systems are a better choice than the SPM-V generator systems for multi-MW direct-drive wind power applications. However, other Vernier machine topologies with improved torque densities and power factors may help to achieve a better overall system level performance than the classical SPM-V machine discussed in this paper. Similarly, any reduction in converter costs in the future due to emerging technologies can make the SPM-V machine even more competitive.

APPENDIX

The numerator and denominator in $\bar{\tau}_r$ presented in (4) can be further expanded as

$$\tau_r = \frac{\pi D_g}{2P_r} \quad (16)$$

$$g = \frac{D_g}{1000} \quad (17)$$

$$h_m = \frac{V_{mag}}{\pi D_g \alpha_p L_{stk}} \quad (18)$$

where D_g and L_{stk} are the airgap diameter and stack length of the machine, V_{mag} is the total magnet volume.

Substituting (16), (17) and (18) in (4), $\bar{\tau}_r$ becomes

$$\bar{\tau}_r = \frac{\pi/(2P_r)}{0.001 + \dfrac{V_{mag}}{\left(\pi D_g{}^2 L_{stk}\right)\alpha_p \mu_{rec}}} \tag{19}$$

Substituting the machine volume in (19) by $V_{mac} = \left(\pi D_g{}^2 L_{stk}\right)/4$, $\bar{\tau}_r$ can be rewritten as

$$\bar{\tau}_r = \frac{\pi/(2P_r)}{0.001 + \left(\dfrac{V_{mag}}{V_{mac}}\right)\dfrac{1}{4\alpha_p \mu_{rec}}} \tag{20}$$

REFERENCES

[1] Z. Zhang, A. Chen, A. Matveev, R. Nilssen, and A. Nysveen, 'High-power generators for offshore wind turbines', *Energy Procedia*, vol. 35, pp. 52–61, Jan. 2013.

[2] D. Li, R. Qu, and J. Li, 'Topologies and analysis of flux-modulation machines', in *Proc. Energy Convers. Congr. Expo. (ECCE)*, Montreal, QC, Canada, Sep. 2015, pp. 2153–2160.

[3] D. W. Li, R. H. Qu, J. Li, L. Y. Xiao, L. L. Wu, and W. Xu, 'Analysis of torque capability and quality in Vernier permanent-magnet machines', *IEEE Trans. Ind. Appl.*, vol. 52, no. 1, pp. 125–135, Jan. 2016.

[4] D. K. Kana Padinharu, G. J. Li, Z. Q. Zhu, M. P. Foster, D. A. Stone, A. Griffo, R. Clark, and A. Thomas, 'Scaling effect on electromagnetic performance of surface mounted permanent magnet Vernier machine', *IEEE Trans. Magn.*, vol. 56, no. 5, pp. 1–15, May 2020.

[5] P. M. Tlali, R. Wang, S. Gerber, C. D. Botha, and M. J. Kamper, 'Design and performance comparison of Vernier and conventional PM synchronous wind generators', *IEEE Trans. Ind. Appl.*, vol. 56, no. 3, pp. 2570–2579, May 2020.

[6] S. Alshibani, V. G. Agelidis, and R. Dutta, 'Lifetime cost assessment of permanent magnet synchronous generators for MW level wind turbines', *IEEE Trans. Sustain. Energy*, vol. 5, no. 1, pp. 10–17, Jan. 2014.

[7] N. A. Bhuiyan and A. McDonald, 'Optimization of offshore direct drive wind turbine generators with consideration of permanent magnet grade and temperature', *IEEE Trans. Energy Convers.*, vol. 34, no. 2, pp. 1105–1114, Jun. 2019.

[8] R. Zeinali and O. Keysan, 'A rare-earth free magnetically geared generator for direct-drive wind turbines', *Energies*, vol. 12, no. 3, p. 447, Jan. 2019.

[9] C. Yicheng, P. Pillay, and A. Khan, 'PM wind generator topologies', *IEEE Trans. Ind. Appl.*, vol. 41, no. 6, pp. 1619–1626, 2005.

[10] A. Toba and T. A. Lipo, 'Generic torque-maximizing design methodology of surface permanent-magnet Vernier machine', *IEEE Trans. Ind. Appl.*, vol. 36, no. 6, pp. 1539–1546, Nov. 2000.

[11] Y. Liu and Z. Q. Zhu, 'Magnetic gearing effect in Vernier permanent magnet synchronous machines', in *IEEE Energy Conversion Congress and Exposition (ECCE)*, Cincinnati, OH, Oct. 2017, pp. 5025–5032.

[12] K. Xie, D. Li, R. Qu, X. Ren, M. R. Shah, and Y. Pan, 'A new perspective on the PM Vernier machine mechanism', *IEEE Trans. Ind. Appl.*, vol. 55, no. 2, pp. 1420–1429, 2019.

[13] A. Grauers, 'Design of direct driven permanent magnet generators for wind turbines', Ph.D. dissertation, Chalmers Univ. Technol., Göteburg, Sweden, 1996.

[14] H. Polinder, F. F. A. van der Pijl, G.- de Vilder, and P. J. Tavner, 'Comparison of direct-drive and geared generator concepts for wind turbines', *IEEE Trans. Energy Convers.*, vol. 21, no. 3, pp. 725–733, Sep. 2006.

[15] H. Li, Z. Chen, and H. Polinder, 'Optimization of multibrid permanent-magnet wind generator systems', *IEEE Trans. Energy Convers.*, vol. 24, no. 1, pp. 82–92, Mar. 2009.

[16] L. Wu, R. Qu, D. Li, and Y. Gao, 'Influence of pole ratio and winding pole numbers on performance and optimal design parameters of surface permanent-magnet Vernier machines', *IEEE Trans. Ind. Appl.*, vol. 51, no. 5, pp. 3707–3715, Sep. 2015.

[17] D. K. P. Kumar, G. J. Li, Z. Q. Zhu, M. P. Foster, D. A. Stone, A. Griffo, M. Odavic, R. Clark, and A. Thomas, 'Influence of demagnetization on selecting the optimum slot/pole number combination for 3MW surface mounted permanent magnet Vernier machine', in *2019 22nd International Conference on Electrical Machines and Systems (ICEMS)*, Harbin, China, Aug. 2019, pp. 1–6.

[18] C. A. da Silva, F. Bidaud, P. Herbet, and J. R. Cardoso, 'Power factor calculation by the finite element method', *IEEE Trans. Magn.*, vol. 46, no. 8, pp. 3002–3005, Aug. 2010.

[19] J. H. J. Potgieter and M. J. Kamper, 'Calculation methods and effects of end-winding inductance and permanent-magnet end flux on performance prediction of nonoverlap winding permanent-magnet machines', *IEEE Trans. Ind. Appl.*, vol. 50, no. 4, pp. 2458–2466, 2014.

[20] L. Wu, R. Qu, and D. Li, 'Analysis of eddy current losses in surface-mounted permanent magnet vernier machines', in *Proc. IEEE Int. Conf. Electr. Mach. Drives*, May 2017, pp. 1–6.

[21] J. R. Hendershot and T. J. E. Miller, *Design of brushless permanent-magnet motors*. Hillsboro, OH: Magna Pysics, 1994.

[22] G. Shrestha, H. Polinder, and J. A. Ferreira, 'Scaling laws for direct drive generators in wind turbines', in *Proc. IEEE Int. Electr. Mach. Drives Conf. (IEMDC)*, May 2009, pp. 797–803.

[23] Z. Q. Zhu and D. Howe, 'Influence of design parameters on cogging torque in permanent magnet machines', *IEEE Trans. Energy Convers.*, vol. 15, no. 4, pp. 407–412, Dec. 2000.

[24] A. Mcdonald and N. Bhuiyan, 'On the optimization of generators for offshore direct drive wind turbines', *IEEE Trans. Energy Convers.*, vol. 32, no. 1, pp. 348–358, Mar. 2017.

[25] H. Polinder, D. Bang, R. P. J. O. M. van Rooij, A. S. McDonald, and M. A. Mueller, '10 MW wind turbine direct-drive generator design with pitch or active speed stall control', in *Proc. IEEE Int. Conf. Electr. Mach. Drives*, Antalya, 2007, vol. 2, pp. 1390–1395, doi: 10.1109/IEMDC.2007.383632.

[26] A. Mcdonald, 'Structural analysis of low speed, high torque electrical generators for direct drive renewable energy converters', PhD dissertation, University of Edinburgh, Edinburgh, 2008.

[27] Z. Zhang, A. Matveev, S. Øvrebø, R. Nilssen, and A. Nysveen, 'State of the art in generator technology for offshore wind energy conversion systems', in *Proc. IEEE Int. Conf. Electr. Mach. Drives*, Niagara Falls, 2011, pp. 1131–1136.

DILEEP KUMAR KANA PADINHARU received his B.Tech. in electrical and electronics engineering from College of Engineering Trivandrum, Kerala, India in 2004 and MSc.(Engg.) in high voltage engineering from Indian Institute of Science Bangalore, India in 2007. He worked for General Electric Company in India from 2007 to 2017, where he was involved in designing high power synchronous generators. Currently, he is pursuing Ph.D. in electrical engineering from the University of Sheffield, U.K. His research interests are design, modelling and optimization of permanent magnet machines.

GUANG-JIN Li (M'10–SM'16) received the B.Eng. degree from Wuhan University, China, in 2007, the M.Sc. degree from the University of Paris XI, France, in 2008, and the Ph.D. degree from the Ecole Normale Supérieure (ENS) de Cachan, Paris, France, in 2011, all in electrical and electronic engineering. He joined the Electrical Machines and Drives (EMD) Group, University of Sheffield, Sheffield, U.K., in 2012, as a Postdoctoral Research Associate, where he was appointed as an Assistant Professor, in 2013. He is currently an Associate Professor in electrical machines with the EMD Group, University of Sheffield. His main research interests include the design, fault analysis, and thermal management of electrical machines for renewable. energy, automotive, and more electrical aircrafts.

ZI-QIANG ZHU (M'90-SM'00-F'09) received the B.Eng. and M.Sc. degrees in electrical and electronic engineering from Zhejiang University, Hangzhou, China, in 1982 and 1984, respectively, and the Ph.D. degree in electronic and electrical engineering from the University of Sheffield, Sheffield, U.K., in 1991.,Since 1988, he has been with the University of Sheffield, where he currently holds the Royal Academy of Engineering/Siemens Research Chair and is the Head of the Electrical Machines and Drives Research Group, the Academic Director of Sheffield Siemens Gamesa Renewable Energy Research Centre, the Director of CRRC Electric Drives Technology Research Centre, and the Director of Midea Electric Machines and Controls Research Centre. His research interests include the design and control of permanent-magnet brushless machines and drives for applications ranging from automotive through domestic appliances to renewable energy. Dr. Zhu is a Fellow of Royal Academy of Engineering.

RICHARD CLARK obtained his B.Eng. degree in Electrical Engineering from the University of Sheffield and received a Ph.D. in 1999 for research on permanent magnet actuators. Following several years as a post-doctoral Research Associate, he was awarded a 5 year Royal Academy of Engineering Research Fellowship and became a Lecturer in Electrical Engineering at the University of Sheffield in 2005. In 2007, he joined Magnomatics, a University of Sheffield spin-out company developing novel electrical motors and generators and magnetic transmissions, where he held posts of R&D Manager, Research Director and Principal Engineer. He joined Siemens Gamesa Renewable Energy Research Centre, Sheffield, U.K as Electromagnetic Specialist in October 2017.

ARWYN THOMAS received the M.Eng. and Ph.D. degrees in electronic and electrical engineering from the University of Sheffield, Sheffield, U.K., in 2005, and 2009, respectively. He is currently with the Sheffield Siemens Gamesa Renewable Energy Research Centre, Sheffield, U.K. His research focuses on the modeling, design and analysis of permanent-magnet brushless machines.

ZIAD AZAR received the B.Eng. degree in electrical engineering from the University of Damascus, Damascus, Syria, in 2003 and M.Sc. degree in electronic and electrical engineering and Ph.D. degree in electrical engineering from The University of Sheffield, Sheffield, U.K., in 2008 and 2012, respectively. His major research interests during his Ph.D. studies included the modelling, design, and analysis of permanent-magnet and magnetless brushless machines for automotive applications. In 2012, Ziad joined Siemens Games Renewable Energy, where he is currently the generator team manager in the technology development department, focus has been on maturing and developing of new technologies for direct-drive wind power generators.